mathematics

MDPI

Article

DeepLabv3+-Based Segmentation and Best Features Selection Using Slime Mould Algorithm for Multi-Class Skin Lesion Classification

Mehwish Zafar [1], Javeria Amin [2,*], Muhammad Sharif [1], Muhammad Almas Anjum [3], Ghulam Ali Mallah [4] and Seifedine Kadry [5,6,7]

1 Department of Computer Science, COMSATS University Islamabad, Wah Campus, Wah Cantt 47040, Pakistan
2 Department of Computer Science, University of Wah, Wah Cantt 47040, Pakistan
3 National University of Technology (NUTECH), Islamabad 44000, Pakistan
4 Department of Computer Science, Shah Abdul Latif University, Khairpur 66111, Pakistan
5 Department of Applied Data Science, Noroff University College, 4612 Kristiansand, Norway
6 Artificial Intelligence Research Center (AIRC), Ajman University, Ajman P.O. Box 346, United Arab Emirates
7 Department of Electrical and Computer Engineering, Lebanese American University, Byblos P.O. Box 13-5053, Lebanon
* Correspondence: javeria.amin@uow.edu.pk

Abstract: The development of abnormal cell growth is caused by different pathological alterations and some genetic disorders. This alteration in skin cells is very dangerous and life-threatening, and its timely identification is very essential for better treatment and safe cure. Therefore, in the present article, an approach is proposed for skin lesions' segmentation and classification. So, in the proposed segmentation framework, pre-trained Mobilenetv2 is utilised in the act of the back pillar of the DeepLabv3+ model and trained on the optimum parameters that provide significant improvement for infected skin lesions' segmentation. The multi-classification of the skin lesions is carried out through feature extraction from pre-trained DesneNet201 with N $\times$ 1000 dimension, out of which informative features are picked from the Slim Mould Algorithm (SMA) and input to SVM and KNN classifiers. The proposed method provided a mean ROC of 0.95 $\pm$ 0.03 on MED-Node, 0.97 $\pm$ 0.04 on PH2, 0.98 $\pm$ 0.02 on HAM-10000, and 0.97 $\pm$ 0.00 on ISIC-2019 datasets.

Keywords: skin cancer; skin segmentation; skin classification; melanoma; DeepLabv3+; CNN

MSC: 68U10

check for updates

Citation: Zafar, M.; Amin, J.; Sharif, M.; Anjum, M.A.; Mallah, G.A.; Kadry, S. DeepLabv3+-Based Segmentation and Best Features Selection Using Slime Mould Algorithm for Multi-Class Skin Lesion Classification. *Mathematics* **2023**, *11*, 364. https://doi.org/10.3390/math11020364

Academic Editors: Miguel Ángel Montero-Alonso and Juan De Dios Luna del Castillo

Received: 18 September 2022
Revised: 28 December 2022
Accepted: 4 January 2023
Published: 10 January 2023

1. Introduction

Skin acts as the most important and massive part of the human body, covering about 20 square feet. The skin plays the role of regulating temperature, allowing the sense of touch, feeling hot and cold, and protecting the inner body from ultraviolet rays [1]. Skin accounts for 15% weight of the whole body, with a surface area of about 2 m^2 [2]. Skin consists of 3 main layers. skin [3]. In skin cancer the rare growing of the skin cell has become uncontrolled [4].In daily routine, some skin cells die, and new cells come on their place [5]. Skin cancer has become common these days. According to the report of cancer statistics estimation in the US in 2021, the new skin cancer (melanoma) estimated score has reached 34,920, where 19,320 are male and 15,600 are female. The death rate estimation is 12,410, with 5570 females and 6840 males [6]. The support of computer-aided diagnosis can motivate dermatologists to develop real-time skin cancer identification algorithms. One of the most essential steps for the analysis of the problem is to extract and select the most prominent and promising features. After that, the designed algorithm must be able to provide better measures than the previous one. The limitation in existing approaches acts as a motivation for the presented work, as semantic segmentation is required to extract the

exact boundaries of the lesion and deep features, and their selection is required for more accurate classification. The main contributions of the presented work are:

- Skin lesions are segmented using the proposed segmentation model, in which features are drawn out through a pre-trained Mobilenetv2 model, which acts as a base of DeepLabv3+ for boundary extraction. The model is attained on the chosen hyperparameters that provide more accurate segmentation results.
- A classification framework is designed in which features are taken through a pre-trained DenseNet-201 model and optimal features are picked using SMA. These optimal features are passed to the machine learning classifier along with labels to perform classification.

2. Related Work

Timely and accurate skin lesion recognition and classification [7,8] is a very important task [9–12]. In the skin lesion analysis segmentation [13,14], it is the most important and second step, coming after pre-processing [15,16]. It divides the image into parts, with these parts being called segments [17]. A hybrid model is proposed which is the combination of k-means with a level set [18,19]. A method is defined in which, segments the input image using k-mean clustering [20,21]. An initial contour edges Chan–Vese model is applied with a genetic algorithm for the recognition of skin lesion boundaries [22,23]. The researcher proposed new pyramid pooling for lesion segmentation [24,25]. A system with Mask-R-CNN is proposed [26,27]. A dense framework is utilised for improvement [28,29]. Segmentation is performed using an adaptive dual attention module [30,31]. An algorithm using Bezier curves used for global optimization [32,33]. The segmentation is performed to accurately discover the lesion using deep learning-based methods, i.e., DeepLab V3+ and Mask R-CNN [34–36]. The encoder is joined with DeepLabV3 and decoder [37,38] for lesion segmentation. Deconvolutional coating are utilised to change the volume of input and output [39,40]. Hierarchical supervision is used to refine the prediction mask [41,42]. To segment, the image fuzzy clustering is utilised [43]. Researchers utilised colour features to partition the image [44–46]. The CNN classification with the novel regularising method proposed provided an accuracy of 0.974 [47]. The ensembles for melanoma classification, are utilised [48,49]. The ARL-CNN classification model is used for effectiveness [50].

3. Proposed Methodology

We developed novel segmentation and classification models. In the proposed segmentation model, a pre-trained Mobilenetv2 model and DeepLabv3+ are utilised. In the proposed classification framework, features are investigated using DesnseNet-201 and novel features are extracted with SMA for multi-classification of skin lesions as presented in Figure 1.

3.1. Segmentation of Skin Lesion

In the proposed segmentation model, features are extracted using Mobilenetv2 [51]. Features obtained from pre-trained Mobilenetv2 are input to the DeepLabv3+ network. DeepLabv3+ [52] is an enhanced version of atrous spatial pyramid pooling, with the addition of image-level features and batch normalization. Atrous convolutional in the last few blocks of the backbone to control the feature map size. The atrous spatial pyramid pooling is added on the peak of taken features that classify every pixel corresponding to their classes. The proposed framework is joined with Mobilenetv2 and Deeplabv3+, which contains 186 layers, in which 01 input, 67 convolutions, 59 batch-norm, 40 flip ReLU, 13 addition, 02 2D-crops, 02 depth concatenation, 01 softmax, and 01 classification layers are included, as illustrated in Figure 2.

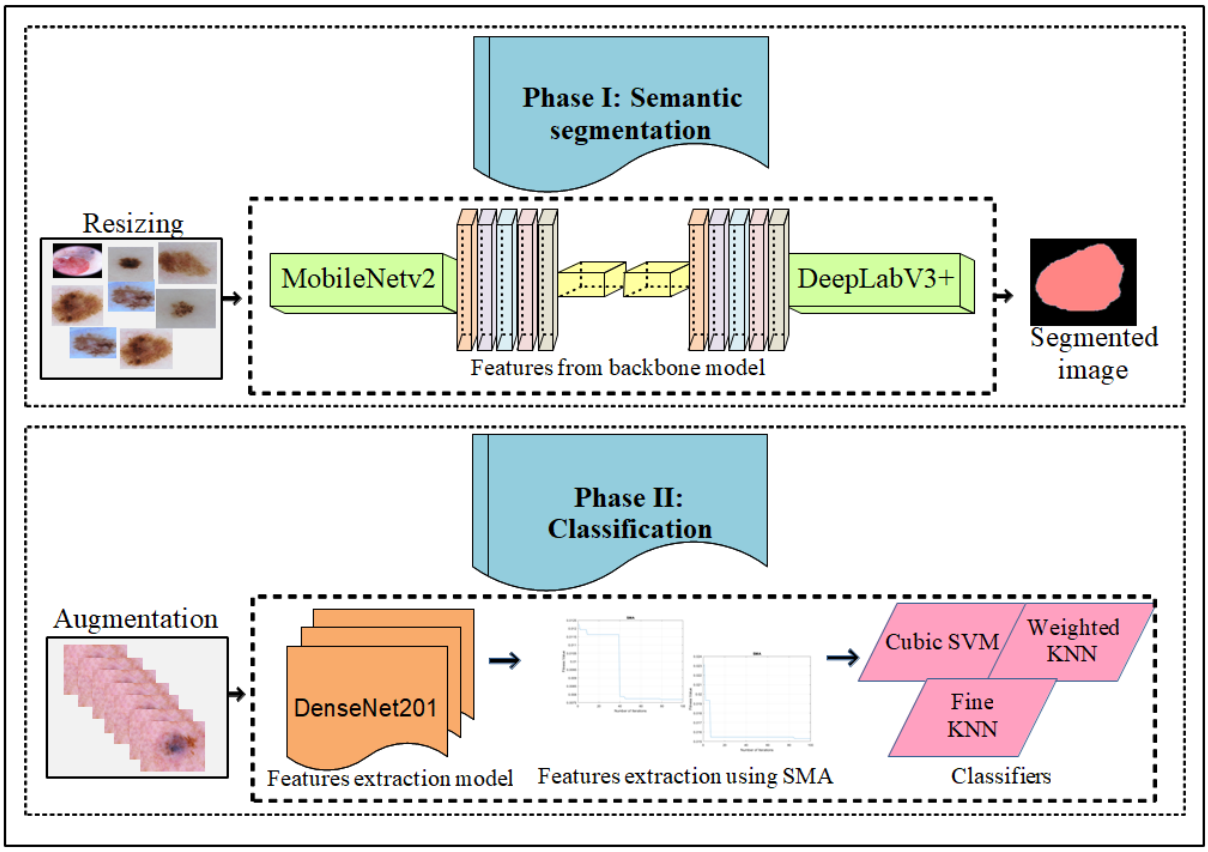

Figure 1. Skin lesions' recognition. Segmentation using Mobilenetv2 and DeepLabv3+; classification based on DenseNet-201 and SMA with SVM, KNN classifiers.

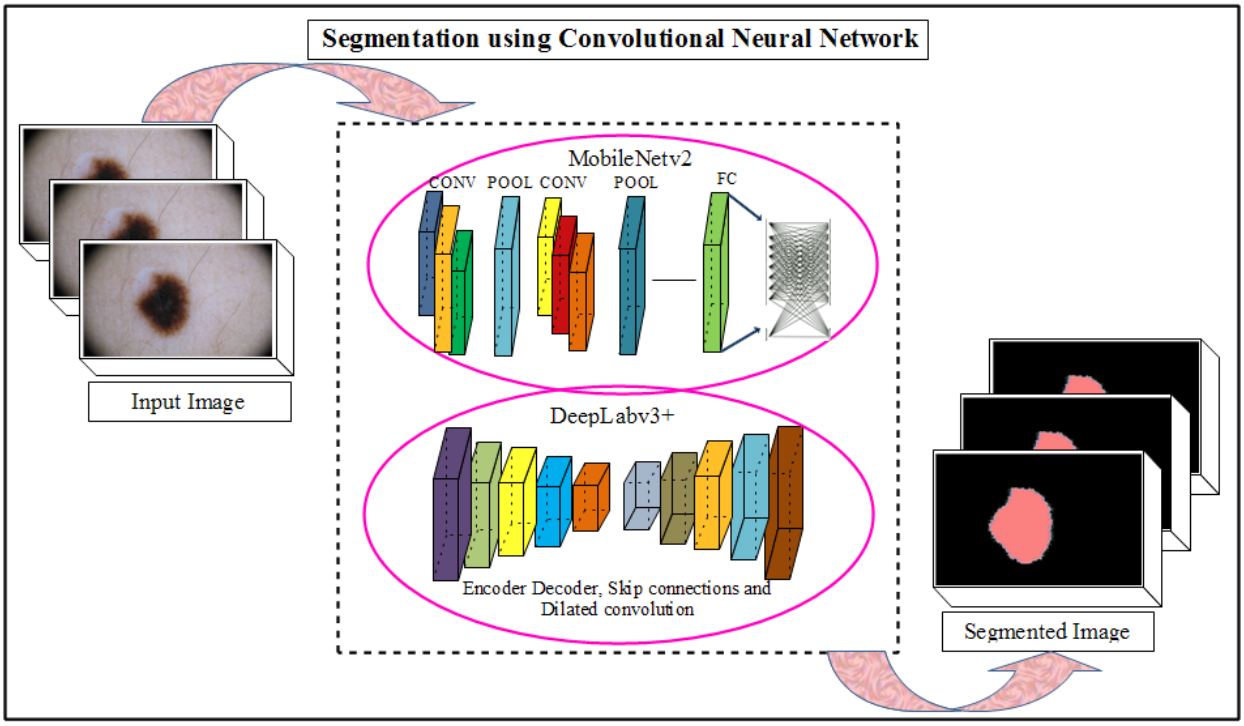

Figure 2. Skin lesions segmentation based on Mobilenet-v2 and Deeplabv3+.

The parameters of segmentation are mentioned in Table 1.

Table 1. Hyper parameters of the proposed framework.

Batch-size	32
Training epochs	100
Rate of learning	0.0001
Optimizer solver	Sgdm

In Table 1, the parameters are concluded after long experimentation, in which 32 batch-size, 100 epochs, 0.0001 rate of learning with sgdm optimizer solver provide good segmentation results.

3.2. Classification of Skin Lesions

The proposed classification model consists of three phases, including features extraction using DenseNet-201, optimal features selection using a slime mould algorithm, and pictorial classification, as in Figure 3.

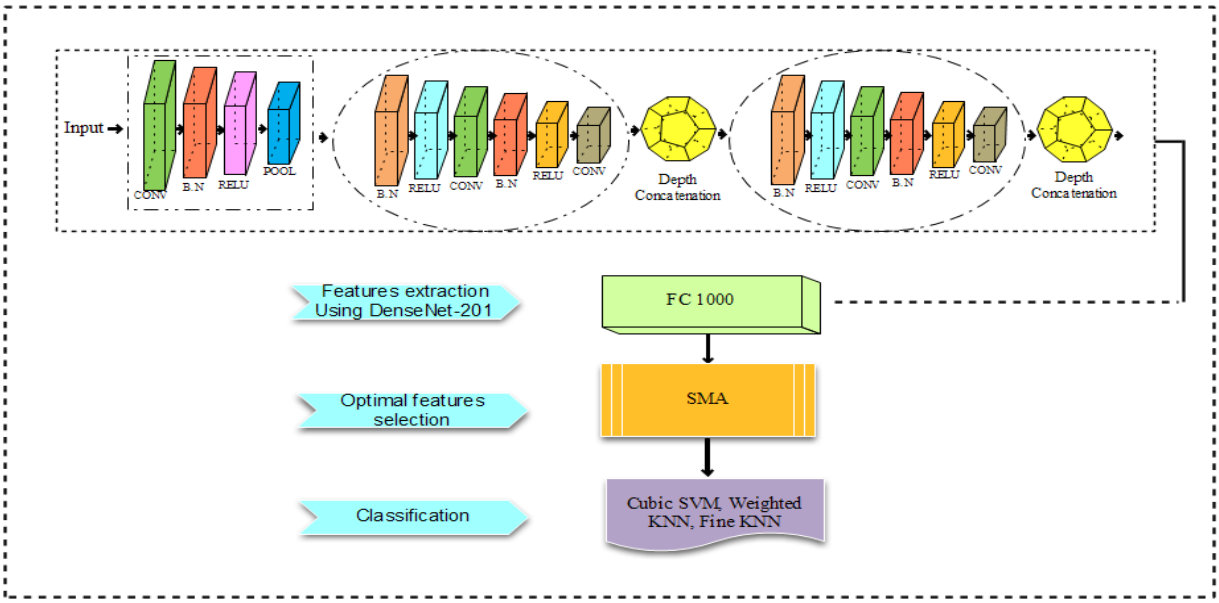

Figure 3. Steps of the proposed classification model.

3.2.1. Features Extraction and Selection

Pre-trained DenseNe-t201 [53,54] model is used to obtain the feature, taken from a fully-connected FC-1000 layer measuring N × 1000, and is input into the slime mould algorithm (SMA) [55]. SMA is an optimization technique used for the best feature selection. SMA [56] is naturally established within slime mould oscillation. Thus, SMA is influenced by the actions of morphological alterations and slime mould. The individual swarms are categorized into three groups. Some of them are picked at the origin, through a proportional number, to be resurrected and carry out their exploration. Some of them pursue their investigation built on their current position and the remaining would be direct towards the foremost candidate. The selected SMA parameters are described in Table 2.

Table 2 depicts the selected parameters of SMA which are utilised for the selection of optimum features, in which the total number of 5 neighbours, 0.2 hold-out validation ratio, the total number of 100 solutions, and maximum 100 iterations are included. The convergence curve in terms of fitness is obtained using SMA, as revealed in Figure 4.

Table 2. Selected parameters of SMA.

Features selection model	SMA
No. of K Nearest Neighbour	Opts.k = 5
Validation data ratio	Ho = 0.2
No. of solutions	Opts. N = 10
Maximum iterations	Opts. T = 100

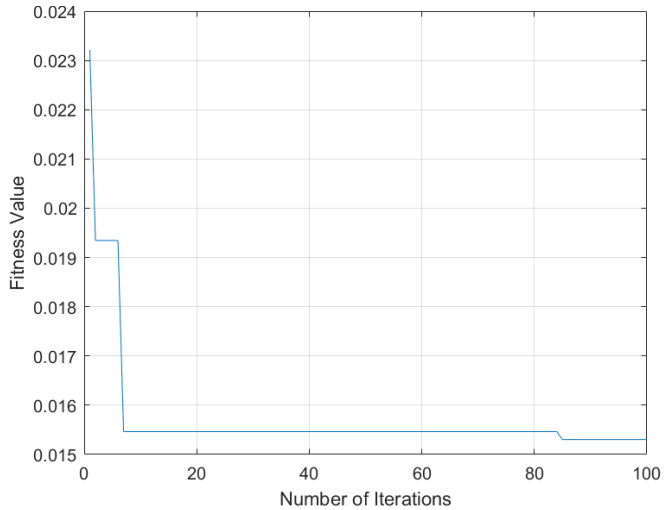

Figure 4. SMA convergence in terms of iterations and fitness value.

The above graph shows the outcomes of the best feature selection on the PH2 dataset using the SMA algorithm. The SMA's mathematical model is discussed below:

$$\overrightarrow{Z}_{(iu+1)} = \begin{cases} \overrightarrow{z_b}(iu) + \overrightarrow{xb} \cdot \left(\overrightarrow{C} \cdot \overrightarrow{Z_A}(iu) - \overrightarrow{Z_B}(iu)\right), & g < h \\ \overrightarrow{gc} \cdot \overrightarrow{Z}(iu), & g \geq h \end{cases} \tag{1}$$

where the $\overrightarrow{xb}$ in Equation (3), $\overrightarrow{gc}$ linearly decreasing towards one to zero. The iu presents the current iteration. The $\overrightarrow{Z_b}$ stands for the current highest accuracy position and it describes the current position, $\overrightarrow{Z}$ defines slime Mould location, $\overrightarrow{z_A}$ and $\overrightarrow{Z_B}$ present randomly selected two individuals from swarms, $\overrightarrow{C}$ defines the weight of slime mould's, and h is shown in Equation (2):

$$h = \tanh |V(j) - eF| \tag{2}$$

where the V (j) shows the fitness of $\overrightarrow{Z}$ where $j \in 1, 2, 3, \ldots n$, and eF define the finest fitness in iterations. The $\overrightarrow{xb}$ is defined as bellow:

$$\overrightarrow{xb} = [-d, d] \tag{3}$$

where the calculation of d is shown in Equation (4)

$$d = \operatorname{arctanh}\left(-\left(\frac{iu}{maximum\_iu}\right) + 1\right) \tag{4}$$

where (maximum iu) shows the maximum iteration.

The $\underset{C}{\rightarrow}$ is presented as follows:

$$\underset{C\ (\text{index}\ (j))}{\rightarrow} = \begin{cases} 1 + g.\log\left(\frac{aF-V(j)}{aF-cF} + 1\right), \text{ Cond.} \\ 1 - g.\log\left(\frac{aF-V\ (j)}{aF-cF} + 1\right), \text{ others} \end{cases} \tag{5}$$

where aF stands for best fitness, cF stands for worst fitness, cond. describes that V (j) categorizes the population in the initial half, g defines a random value between [0, 1] interval. Index defines sorted values of fitness and computed, as described in Equation (6).

$$\text{index} = \text{Sort (V)} \tag{6}$$

The uncertainty is described in Equation (5), simulated using r. The log decreased the change rate of numerical values; therefore, not too many changes occur in frequency.

The slime mould changes its search pattern, conforming to the nature of the worth of the food. When the mass is greater, food concentration becomes sufficient, and the mass should decrease when the food concentration becomes poor, as presented in Equation (7).

$$\underset{z^*}{\rightarrow} = \begin{cases} \text{random}\cdot\ (ub - lb) + lb, & \text{random}\ < k \\ \underset{Z_b(iu)}{\rightarrow} + \underset{Xb}{\rightarrow} \cdot (\underset{C}{\rightarrow} \cdot \underset{Z_A(iu)}{\rightarrow} - \underset{Z_B(iu)}{\rightarrow}), & g < h \\ \underset{gc}{\rightarrow} \cdot \underset{Z(iu),}{\rightarrow} & g\ \geq h \end{cases} \tag{7}$$

where the ub and lb define the upper and lower boundaries, and g defines the random value of 0 and 1. Figure 5 depicts the optimization process of the feature vector.

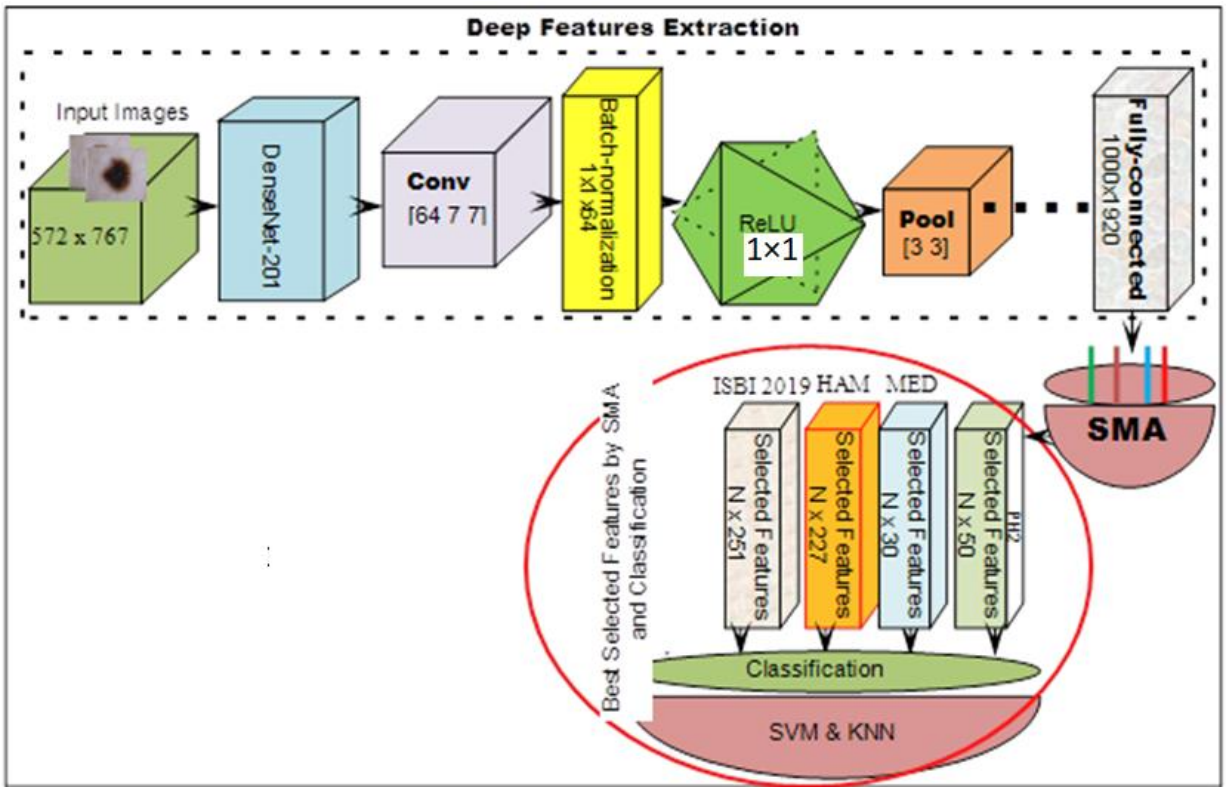

Figure 5. Optimal features selection using SMA.

Table 3 depicts the selected feature vector dimensions after applying SMA.

Table 3. Selected numbers of features in each dataset.

Datasets	Total Features	No. of Selected Features
PH2	N × 1000	N × 50
MED-NODE		N × 30
HAM10000		N × 227
ISIC 2019		N × 251

Table 3 shows the best-selected features number on PH2, MED-NODE, HAM10000, and ISIC 2019 datasets in both the training and testing phases.

3.2.2. Classification Using Selected Classifiers

The classifier takes the value of numerous features to make a prediction and consists of the number of parameters that it should learn from training data. The learned classifier shows the correspondence between the labels in training data and features [57]. In the proposed methodology, by using optimal features, the three classifiers have been utilised to differentiate the skin lesions into relevant classes.

The cubic kernel SVM [58] and its chosen parameters are stated in Table 4.

Table 4. Parameters of SVM.

Model	Cubic SVM
Function of Kernel	Cubic
Scale of Kernel	Automatic
Level of box constraint	01
Multiclass method	One-vs-One
Data Standardization	True

For classification purposes, the weighted KNN [59] and fine KNN [60] selected parameters are presented in Table 5.

Table 5. Parameters of KNN classifier.

Model	Fine KNN	Weighted KNN
No. of neighbours	1	10
Metric of distance	Euclidean	Euclidean
Distance weight	Equal	Square inverse
Data Standardization	True	True

4. Experimental Discussion/Setup

The achievement of the proposed segmentation approach is estimated on four public datasets ISIC 2016 [61], 2017 [62], 2018 [63], and PH2 [64,65]. The four public datasets ISIC 2019 [66,67], HAM10000 [66], PH2 [64], and MED-NODE [68,69] were utilised to estimate the performance of the proposed classification framework after augmentation. MATLAB 2020b is utilised as an implementation tool, using Intel core i5 6th Generation hardware on Windows 10.

4.1. Experiment#1: Segmentation

The proposed segmentation approach performance is computed based on global accuracy, mean Accuracy, meanIoU, weightedIoU, and mean BF score using ISIC 2016,17,18, and PH2 datasets, as shown in Table 6.

Table 6. Skin lesion segmentation performance on ISIC-2016, 2017, 2018, and PH2 datasets.

Dataset	Global Accuracy	Mean Accuracy	Mean IoU	Weighted IoU	Mean BF Score
ISIC 2016	0.97481	0.96253	0.93960	0.95082	0.88649
ISIC 2017	0.97297	0.96841	0.94483	0.94724	0.84741
ISIC 2018	0.98642	0.91472	0.88139	0.97390	0.78364
PH2	0.95914	0.96005	0.90477	0.92299	0.82448

Table 6 depicts the proposed segmentation results, in which we achieved a global accuracy of 0.97481, 0.97297, 0.98642, 0.95914 on ISIC 2016, 2017, 2018, and PH2, respectively. The proposed framework segmentation outcomes using benchmark ISIC 2016 and PH2 datasets are stated in Figures 6 and 7.

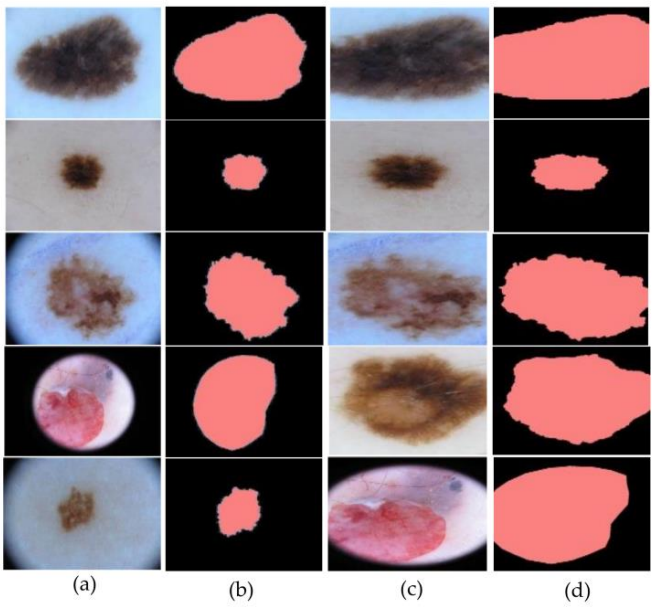

Figure 6. Visualisation results (**a**) input image of ISIC 2016 (**b**) segmented output of ISIC 2016 (**c**) input image of ISIC 2017 (**d**) segmented output of ISIC 2017.

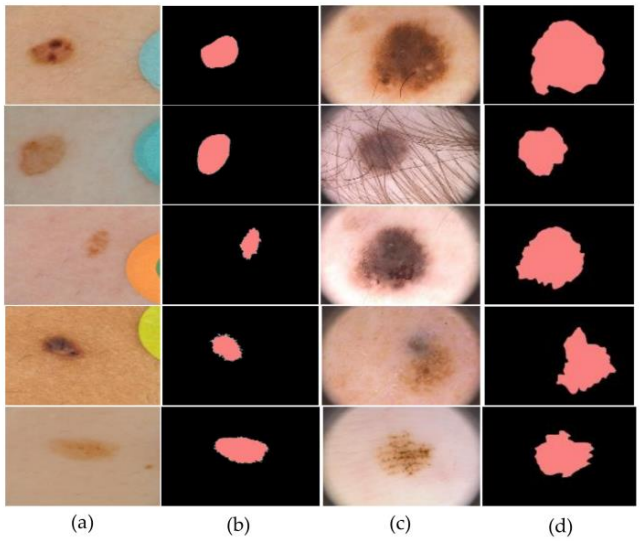

Figure 7. Visualisation results (**a**) input image of ISIC 2018 (**b**) segmented output of ISIC 2018 (**c**) input image of PH2 (**d**) segmented output of PH2.

The achieved results are also compared to existing research work, as presented in Table 7.

Table 7. Comparison of the existing research works on similar datasets.

Ref#	Year	Datasets	Accuracy
[70]	2022	ISIC 2016	96%
[71]	2021		95.4%
[22]	2021		96.2%
[72]	2020		93.8%
[32]	2020		95.24%
[73]	2019		95.78%
Proposed Method			97.48%
[70]	2022	ISIC 2017	95%
[71]	2021		92.6%
[72]	2020		93.8%
[74]	2020		95.14%
[75]	2020		94.58
[76]	2018		94.03%
Proposed Method			97.29%
[77]	2022	ISIC 2018	97.39
[28]	2021		96.95%
[78]	2021		95.0%
[30]	2020		94.7%
[79]	2019		96.23
[80]	2018		96.80%
Proposed Method			98.64%
[81]	2022	PH2	95.14
[71]	2021		94.3%
[18]	2021		94.6%
[72]	2020		94.9%
[32]	2020		93.2%
[82]	2019		93.1%
Proposed Method			95.91%

On the 2016 challenge dataset, the existing technique provides a maximum of 96.2% accuracy using GA-based optimization [22]. On the 2017 segmentation challenging dataset, FC-DPN provides 95.14% accuracy but some lesions are not segmented accurately due to blurry and low-contrast images [74]. The w-net model provides 97.39% accuracy of segmentation, though an improvement is required in the deep learning framework to increase the segmentation results [77]. Antialiasing convolution model is utilised for skin lesion segmentation, providing 95% prediction scores. The segmentation scores might be increased using the improved features optimization approach [70].

The proposed method in this article consists of Mobilenetv2 and DeepLabv3+, which detects lesion boundaries more accurately, with an accuracy of 97.48%, 97.29%, 98.64% and 95.91% on challenge 2016, 17, 18 and PH2, respectively, making it far more efficient compared to the existing work.

4.2. Experiment#2: Skin Lesions Classification

In the classification experiment, features are computed using pre-trained DenseNet-201 and selected optimum features by SMA that are supplied to the classifiers on 5-fold cross-validation. The graphical depiction of the proposed classification results is expressed in Figures 8–11. The classification results are described in Table 8.

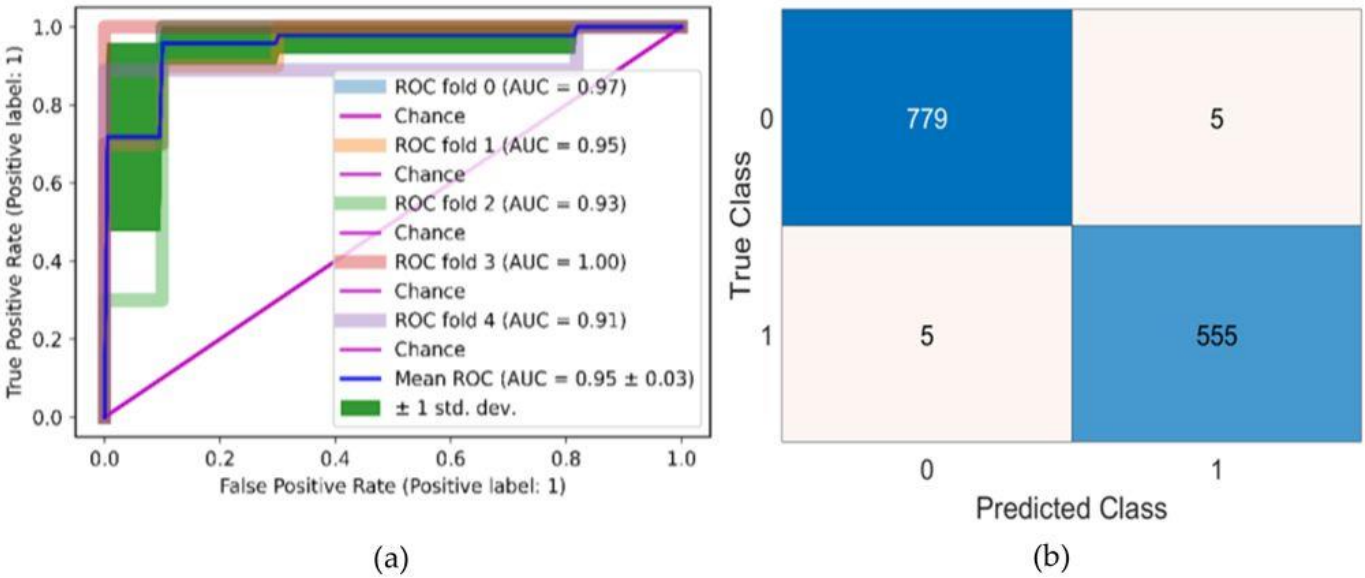

Figure 8. Classification results on MED-NODE (**a**) ROC curve of fine KNN (**b**) confusion matrix of fine KNN.

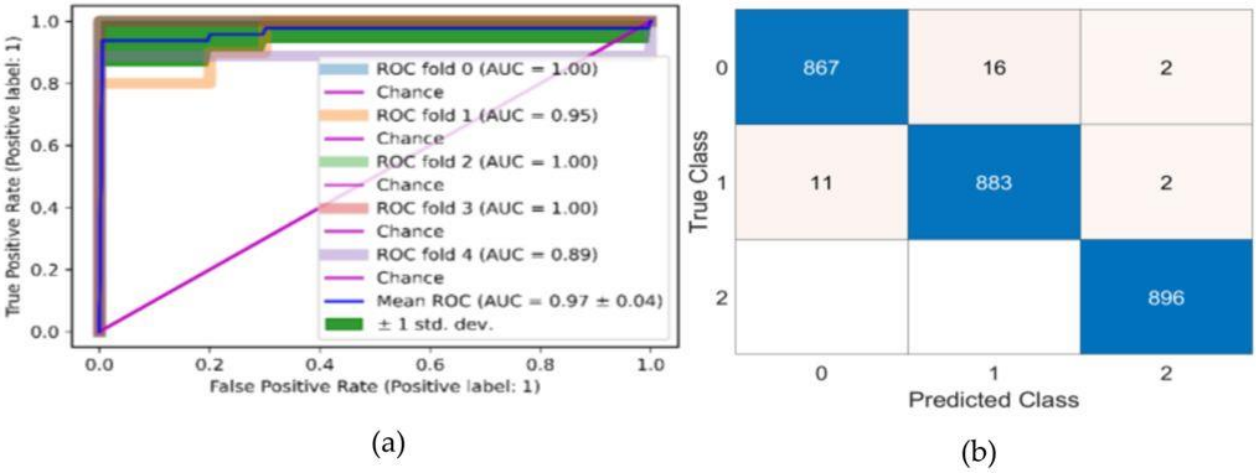

Figure 9. Classification results on PH2 (**a**) ROC curve of fine KNN (**b**) confusion matrix of fine KNN.

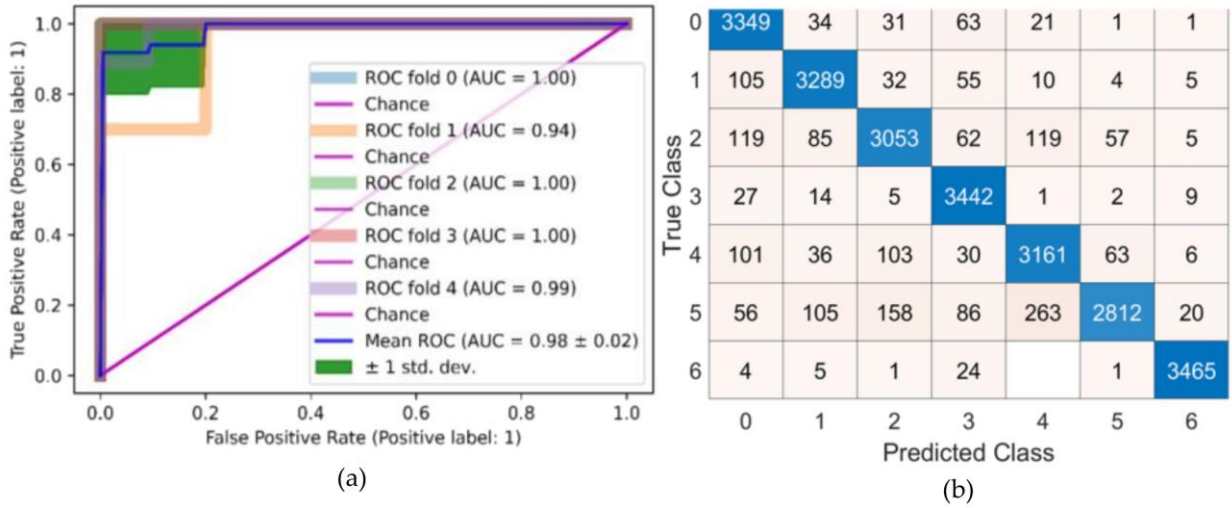

Figure 10. Classification results on HAM10000 (**a**) ROC curve of fine KNN (**b**) confusion matrix of fine KNN.

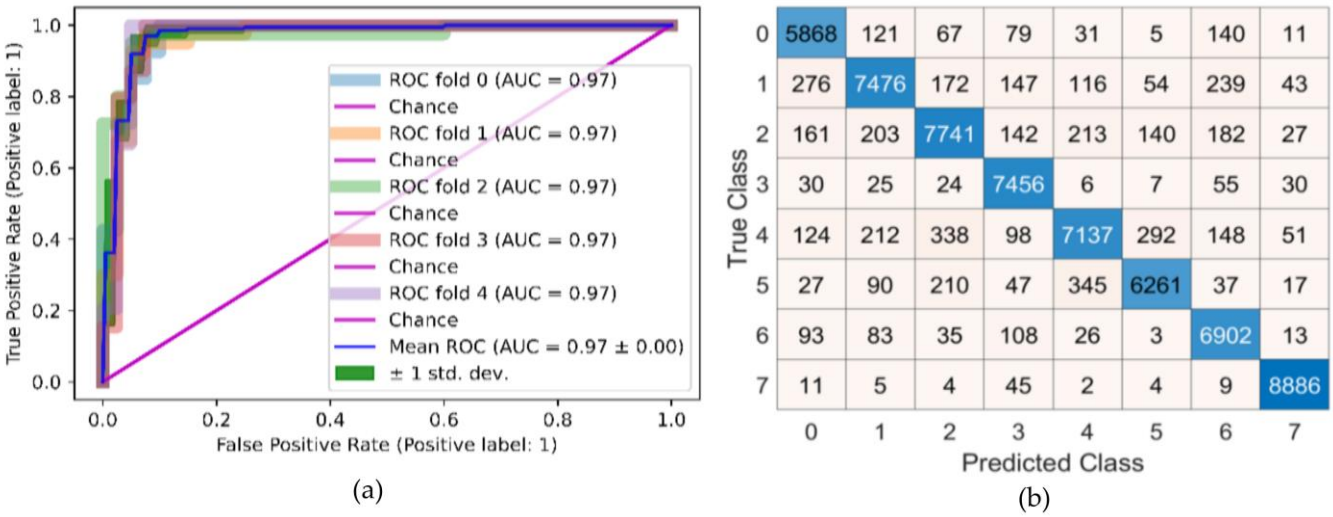

Figure 11. Classification results on ISIC 2019 (**a**) ROC Curve of fine KNN (**b**) confusion matrix of fine KNN.

Table 8. Proposed classification model outcomes on the MED-NODE dataset.

Classifiers	Classes		Accuracy	Precision	Recall	F1 Score	Overall Accuracy
	Melanoma (M)	Nevus (N)					
Cubic SVM	✓		97.32%	0.98	0.97	0.98	97.87%
		✓	97.32%	0.96	0.97	0.97	
Weighted KNN	✓		97.62%	0.99	0.97	0.98	97.62%
		✓	97.62%	0.96	0.98	0.97	
Fine KNN	✓		99.33%	0.99	0.99	0.99	99.33%
		✓	99.33%	0.99	0.99	0.99	

As given in Table 8, the classification of the MED-NODE dataset was performed using three classifiers: cubic SVM, weighted KNN, and fine KNN, with an overall accuracy of 97.32%, 97.62%, and 99.33%, respectively. All the classifiers were trained using

cross-validation 5 folds dataset distribution. The classification outcomes on the PH2 are mentioned in Table 9.

Table 9. Proposed classification model results on PH2.

Classifiers	Classes			Accuracy	Precision	Recall	F1 Score	Overall Accuracy
	AN	CN	M					
Cubic SVM	✓			97.95%	0.97	0.97	0.97	97.87%
		✓		98.06%	0.97	0.97	0.97	
			✓	99.74%	1.00	1.00	1.00	
Weighted KNN	✓			98.17%	0.97	0.98	0.97	98.09%
		✓		98.43%	0.98	0.97	0.98	
			✓	99.59%	1.00	0.99	0.99	
Fine KNN	✓			98.99%	0.98	0.99	0.98	98.88%
		✓		98.92%	0.99	0.98	0.98	
			✓	99.85%	1.00	1.00	1.00	

In Table 9, cubic SVM achieved an accuracy of 97.87%. The results of the weighted KNN and fine KNN classifiers are 98.09% and 98.88%, respectively. The classification outcomes on the HAM10000 are mentioned in Table 10.

Table 10. Proposed classification model results on HAM10000.

Classifiers	Classes							Accuracy	Precision	Recall	F1 Score	Overall Accuracy
	AK	BCC	BK	D	M	N	VL					
Cubic SVM	✓							97.18%	0.92	0.89	0.90	90.65%
		✓						97.35%	0.92	0.90	0.91	
			✓					95.67%	0.84	0.86	0.85	
				✓				98.93%	0.97	0.96	0.96	
					✓			95.57%	0.84	0.85	0.84	
						✓		96.91%	0.87	0.91	0.89	
							✓	99.68%	0.99	0.99	0.99	
Weighted KNN	✓							95.89%	0.94	0.80	0.87	86.96%
		✓						96.49%	0.89	0.86	0.88	
			✓					94.55%	0.71	0.88	0.79	
				✓				97.22%	0.99	0.84	0.91	
					✓			94.73%	0.80	0.82	0.81	
						✓		95.67%	0.77	0.91	0.83	
							✓	99.38%	0.98	0.98	0.98	
Fine KNN	✓							97.67%	0.95	0.89	0.92	92.01%
		✓						98.02%	0.94	0.92	0.93	
			✓					96.74%	0.87	0.90	0.88	
				✓				98.36%	0.98	0.91	0.95	
					✓			96.82%	0.89	0.88	0.89	
						✓		96.69%	0.81	0.96	0.87	
							✓	99.7%	0.99	0.99	0.99	

Table 11 shows the outcomes of the cubic SVM, weighted KNN, and fine KNN, which obtained an overall accuracy of 90.65%, 86.90%, and 92.01%, respectively. The classification outcomes of the ISIC 2019 are depicted in Table 11.

Table 11. Classification results on ISIC 2019 dataset.

Classifiers	Classes								Accuracy	Precision	Recall	F1 Score	Overall Accuracy
	AK	BCC	BK	D	M	MN	SCC	VL					
Cubic SVM	✓								97.58%	0.88	0.88	0.88	89.99%
		✓							96.81%	0.89	0.88	0.88	
			✓						95.81%	0.84	0.86	0.85	
				✓					98.76%	0.96	0.94	0.95	
					✓				96.23%	0.83	0.88	0.85	
						✓			97.77%	0.90	0.90	0.90	
							✓		97.37%	0.91	0.87	0.89	
								✓	97.77%	0.91	0.87	0.89	
Weighted KNN	✓								96.65%	0.86	0.88	0.87	90.22%
		✓							96.44%	0.83	0.91	0.87	
			✓						98.17%	0.98	0.88	0.93	
				✓					96.4%	0.82	0.90	0.86	
					✓				97.93%	0.90	0.91	0.91	
						✓			97.67%	0.94	0.87	0.90	
							✓		99.41%	0.99	0.97	0.98	
								✓	97.77%	0.91	0.87	0.89	
Fine KNN	✓								98.13%	0.93	0.89	0.91	91.7%
		✓							97.16%	0.88	0.91	0.89	
			✓						96.95%	0.88	0.90	0.89	
				✓					98.66%	0.98	0.92	0.95	
					✓				96.82%	0.85	0.91	0.88	
						✓			97.97%	0.89	0.93	0.91	
							✓		98.14%	0.95	0.89	0.92	
								✓	99.57%	0.99	0.98	0.98	

Table 11 shows the outcomes of the cubic SVM, weighted KNN, and fine KNN with an overall accuracy of 89.99%, 90.22%, and 91.7%. The result shows that fine KNN performs best among the three classifiers. The classification results comparison is mentioned in Table 12.

In Table 12, the classification results with existing methods using ISIC 2019, HAM10000, PH2, and MED-NODE datasets are shown. On dataset ISIC 2019, deep learning and an entropy-based approach provided 91% accuracy; however, there is still room to improve the model for better accuracy [83]. On the HAM-10000 dataset, the accuracy rate achieved is 89.8% based on deep features extraction and selection approach [89]. On the dataset PH2, 97.5% accuracy is achieved using a combination of deep and texture features. The classification results might be increased using shape and colour features [91]. On MED-NODE dataset, the accuracy is 97.70% using transfer learning model [69].

Table 12. Comparisons of proposed classification method outcomes with existing approaches.

Ref#	Year	Datasets	Accuracy
[83]	2019	ISIC 2019	91%
[84]	2020		84.79%
[85]	2020		82.5%
Proposed			*91.7%*
[86]	2022	HAM10000	80%
[87]	2021		85.50%
[88]	2021		88.50%
[89]	2019		89.8%
Proposed			*92.01%*
[90]	2022	PH2	94.97%
[91]	2021		97.5%
[92]	2020		96.9%
[93]	2020		85.7%
[94]	2020		94.0
Proposed			*98.88%*
[90]	2022	MED-NODE	92%
[95]	2021		97%
[96]	2020		83.33%
[69]	2019		97.70%
Proposed			*99.33%*

In this research, however, features from the selected layers of the pre-trained models and the best features are selected using an SMA model that provides an accuracy of 91.7% on ISIC 2019, 92.01% on HAM10000, 98.88% on PH2, and 99.33% on MED-NODE datasets. The experimental outcomes show that the achieved outcomes are finer compared to the newest works in this domain.

5. Conclusions

Skin lesions' detection is a complex job due to resemblances among the classes of skin lesions. To overcome the existing challenge, novel deep learning models are designed for skin lesion analysis. To perform semantic segmentation, the deep features are taken through the pre-trained model Mobilenetv2, which are then passed to the DeepLabv3+ for the extraction of the exact border of the lesion. The proposed segmentation approach is evaluated based on Mean Accuracy, Global Accuracy, BF Score, Weighted IoU, and Mean IoU on ISIC 2016, 2017, 2018, and PH2 datasets, which provide a global accuracy of 0.97481, 0.97297, 0.98642, and 0.95914, respectively.

In the proposed classification model, deep features are taken using DenseNet-201, and select optimal features by SMA, which are then evaluated on the MED-NODE, PH2, HAM-10000, and ISIC 2019 benchmark datasets, providing an accuracy of 99.33%, 98.88%, 92.01%, and 91.7, respectively. The achieved outcomes of segmentation and classification are far better compared to existing techniques.

Author Contributions: Conceptualization, M.Z. and J.A.; Methodology, M.S., G.A.M. and S.K.; Formal analysis, M.A.A. All authors have read and agreed to the published version of the manuscript.

Funding: This research received no external funding.

Data Availability Statement: Not applicable.

Conflicts of Interest: The authors declare no conflict of interest.

References

1. Hameed, N.; Ruskin, A.; Hassan, K.A.; Hossain, M.A. A comprehensive survey on image-based computer aided diagnosis systems for skin cancer. In Proceedings of the 2016 10th International Conference on Software, Knowledge, Information Management & Applications (SKIMA), Chengdu, China, 15–17 December 2016.
2. Lai-Cheong, J.E.; McGrath, J.A. Structure and function of skin, hair and nails. *Medicine* **2013**, *41*, 317–320. [CrossRef]
3. Gordon, R. Skin cancer: An overview of epidemiology and risk factors. *Semin. Oncol. Nurs.* **2013**, *29*, 160–169. [CrossRef] [PubMed]
4. Javed, R.; Rahim, M.S.M.; Saba, T.; Rehman, A. A comparative study of features selection for skin lesion detection from dermoscopic images. *Netw. Model. Anal. Heal. Inform. Bioinform.* **2019**, *9*, 4.
5. Zhang, N.; Cai, Y.-X.; Wang, Y.-Y.; Tian, Y.-T.; Wang, X.-L.; Badami, B. Skin cancer diagnosis based on optimized convolutional neural network. *Artif. Intell. Med.* **2020**, *102*, 101756. [CrossRef] [PubMed]
6. Key Statistics for Melanoma Skin Cancer. Available online: https://www.cancer.org/cancer/melanoma-skin-cancer/about/key-statistics.html (accessed on 12 October 2021).
7. Shetty, B.; Fernandes, R.; Rodrigues, A.P.; Chengoden, R.; Bhattacharya, S.; Lakshmanna, K. Skin lesion classification of dermoscopic images using machine learning and convolutional neural network. *Sci. Rep.* **2022**, *12*, 18134. [CrossRef]
8. Liang, Y.; Sun, L.; Ser, W.; Lin, F.; Thng, S.T.G.; Chen, Q.; Lin, Z. Classification of non-tumorous skin pigmentation disorders using voting based probabilistic linear discriminant analysis. *Comput. Biol. Med.* **2018**, *99*, 123–132. [CrossRef]
9. Amin, J.; Sharif, M.; Raza, M.; Saba, T.; Rehman, A. Brain tumor classification: Feature fusion. In Proceedings of the 2019 International Conference on Computer and Information Sciences (ICCIS), Sakaka, Saudi Arabia, 3–4 April 2019.
10. Amin, J.; Sharif, M.; Yasmin, M.; Saba, T.; Raza, M. Use of machine intelligence to conduct analysis of human brain data for detection of abnormalities in its cognitive functions. *Multimed. Tools Appl.* **2020**, *79*, 10955–10973. [CrossRef]
11. Amin, J.; Almas-Anjum, M.; Sharif, M.; Kadry, S.; Nam, Y. Fruits and vegetable diseases recognition using convolutional neural networks. *Comput. Mater. Contin.* **2021**, *70*, 619–635. [CrossRef]
12. Saleem, S.; Amin, J.; Sharif, M.; Anjum, M.A.; Iqbal, M.; Wang, S.-H. A deep network designed for segmentation and classification of leukemia using fusion of the transfer learning models. *Complex Intell. Syst.* **2022**, *8*, 3105–3120. [CrossRef]
13. Wei, Z.; Shi, F.; Song, H.; Ji, W.; Han, G. Attentive boundary aware network for multi-scale skin lesion segmentation with adversarial training. *Multimed. Tools Appl.* **2020**, *79*, 27115–27136. [CrossRef]
14. Wei, Z.; Song, H.; Li, L.; Chen, Q.; Han, G. Attention-based DenseUnet network with adversarial training for skin lesion segmentation. *IEEE Access* **2019**, *7*, 136616–136629. [CrossRef]
15. Sharif, M.I.; Li, J.P.; Amin, J.; Sharif, A. An improved framework for brain tumor analysis using MRI based on YOLOv2 and convolutional neural network. *Complex Intell. Syst.* **2021**, *7*, 2023–2036. [CrossRef]
16. Sharif, M.; Amin, J.; Raza, M.; Yasmin, M.; Satapathy, S.C. An integrated design of particle swarm optimization (PSO) with fusion of features for detection of brain tumor. *Pattern Recognit. Lett.* **2020**, *129*, 150–157. [CrossRef]
17. Saba, T.; Mohamed, A.S.; El-Affendi, M.; Amin, J.; Sharif, M. Brain tumor detection using fusion of hand crafted and deep learning features. *Cogn. Syst. Res.* **2020**, *59*, 221–230. [CrossRef]
18. Hwang, Y.N.; Seo, M.J.; Kim, S.M. A segmentation of melanocytic skin lesions in dermoscopic and standard images using a hybrid two-stage approach. *BioMed Res. Int.* **2021**, *2021*, 5562801. [CrossRef]
19. Amin, J.; Sharif, M.; Gul, N.; Yasmin, M.; Shad, S.A. Brain tumor classification based on DWT fusion of MRI sequences using convolutional neural network. *Pattern Recognit. Lett.* **2020**, *129*, 115–122. [CrossRef]
20. Garg, S.; Jindal, B. Skin lesion segmentation using k-mean and optimized fire fly algorithm. *Multimed. Tools Appl.* **2021**, *80*, 7397–7410. [CrossRef]
21. Amin, J.; Sharif, A.; Gul, N.; Anjum, M.A.; Nisar, M.W.; Azam, F.; Bukhari, S.A.C. Integrated design of deep features fusion for localization and classification of skin cancer. *Pattern Recognit. Lett.* **2020**, *131*, 63–70. [CrossRef]
22. Ashour, A.S.; Nagieb, R.M.; El-Khobby, H.A.; Abd-Elnaby, M.M.; Dey, N. Genetic algorithm-based initial contour optimization for skin lesion border detection. *Multimed. Tools Appl.* **2021**, *80*, 2583–2597. [CrossRef]
23. Amin, J.; Sharif, M.; Gul, N.; Raza, M.; Anjum, M.A.; Nisar, M.W.; Bukhari, S.A.C. Brain tumor detection by using stacked autoencoders in deep learning. *J. Med. Syst.* **2020**, *44*, 32. [CrossRef]
24. Kaur, R.; GholamHosseini, H.; Sinha, R.; Lindén, M. Automatic lesion segmentation using atrous convolutional deep neural networks in dermoscopic skin cancer images. *BMC Med. Imaging* **2022**, *22*, 103. [CrossRef]
25. Sharif, M.; Amin, J.; Raza, M.; Anjum, M.A.; Afzal, H.; Shad, S.A. Brain tumor detection based on extreme learning. *Neural Comput. Appl.* **2020**, *32*, 15975–15987. [CrossRef]
26. Bagheri, F.; Tarokh, M.J.; Ziaratban, M. Skin lesion segmentation from dermoscopic images by using Mask R-CNN, Retina-Deeplab, and graph-based methods. *Biomed. Signal Process. Control.* **2021**, *67*, 102533. [CrossRef]
27. Amin, J.; Sharif, M.; Rehman, A.; Raza, M.; Mufti, M.R. Diabetic retinopathy detection and classification using hybrid feature set. *Microsc. Res. Tech.* **2018**, *81*, 990–996. [CrossRef] [PubMed]
28. Qamar, S.; Ahmad, P.; Shen, L. Dense encoder-decoder–based architecture for skin lesion segmentation. *Cogn. Comput.* **2021**, *13*, 583–594. [CrossRef]

29. Amin, J.; Sharif, M.; Anjum, M.A.; Raza, M.; Bukhari, S.A.C. Convolutional neural network with batch normalization for glioma and stroke lesion detection using MRI. *Cogn. Syst. Res.* **2020**, *59*, 304–311. [CrossRef]
30. Wu, H.; Pan, J.; Li, Z.; Wen, Z.; Qin, J. Automated skin lesion segmentation via an adaptive dual attention module. *IEEE Trans. Med. Imaging* **2020**, *40*, 357–370. [CrossRef]
31. Muhammad, N.; Sharif, M.; Amin, J.; Mehboob, R.; Gilani, S.A.; Bibi, N.; Javed, H.; Ahmed, N. Neurochemical alterations in sudden unexplained perinatal deaths—A review. *Front. Pediatr.* **2018**, *6*, 6. [CrossRef] [PubMed]
32. Abdulhamid, I.A.M.; Sahiner, A.; Rahebi, J. New auxiliary function with properties in nonsmooth global optimization for melanoma skin cancer segmentation. *BioMed Res. Int.* **2020**, *2020*, 5345923. [CrossRef]
33. Sharif, M.; Amin, J.; Nisar, M.W.; Anjum, M.A.; Muhammad, N.; Shad, S.A. A unified patch based method for brain tumor detection using features fusion. *Cogn. Syst. Res.* **2020**, *59*, 273–286. [CrossRef]
34. Goyal, M.; Oakley, A.; Bansal, P.; Dancey, D.; Yap, M.H. Skin lesion segmentation in dermoscopic images with ensemble deep learning methods. *IEEE Access* **2019**, *8*, 4171–4181. [CrossRef]
35. Sharif, M.; Amin, J.; Siddiqa, A.; Khan, H.U.; Malik, M.S.A.; Anjum, M.A.; Kadry, S. Recognition of different types of leukocytes using YOLOv2 and optimized bag-of-features. *IEEE Access* **2020**, *8*, 167448–167459. [CrossRef]
36. Anjum, M.A.; Amin, J.; Sharif, M.; Khan, H.U.; Malik, M.S.A.; Kadry, S. Deep semantic segmentation and multi-class skin lesion classification based on convolutional neural network. *IEEE Access* **2020**, *8*, 129668–129678. [CrossRef]
37. Lameski, J.; Jovanov, A.; Zdravevski, E.; Lameski, P.; Gievska, S. Skin lesion segmentation with deep learning. In Proceedings of the IEEE EUROCON 2019-18th International Conference on Smart Technologies, Novi Sad, Serbia, 1–4 July 2019.
38. Sharif, M.; Amin, J.; Yasmin, M.; Rehman, A. Efficient hybrid approach to segment and classify exudates for DR prediction. *Multimed. Tools Appl.* **2020**, *79*, 11107–11123. [CrossRef]
39. Amin, J.; Sharif, M.; Gul, E.; Nayak, R.S. 3D-semantic segmentation and classification of stomach infections using uncertainty aware deep neural networks. *Complex Intell. Syst.* **2022**, *8*, 3041–3057. [CrossRef]
40. Amin, J.; Anjum, M.A.; Sharif, M.; Saba, T.; Tariq, U. An intelligence design for detection and classification of COVID-19 using fusion of classical and convolutional neural network and improved microscopic features selection approach. *Microsc. Res. Tech.* **2021**, *84*, 2254–2267. [CrossRef]
41. Li, H.; He, X.; Zhou, F.; Yu, Z.; Ni, D.; Chen, S.; Wang, T.; Lei, B. Dense deconvolutional network for skin lesion segmentation. *IEEE J. Biomed. Health Inform.* **2018**, *23*, 527–537. [CrossRef]
42. Amin, J.; Sharif, M.; Anjum, M.A.; Khan, H.U.; Malik, M.S.A.; Kadry, S. An integrated design for classification and localization of diabetic foot ulcer based on CNN and YOLOv2-DFU models. *IEEE Access* **2020**, *8*, 228586–228597. [CrossRef]
43. Amin, J.; Sharif, M.; Yasmin, M. Segmentation and classification of lung cancer: A review. *Immunol. Endocr. Metab. Agents Med. Chem.* **2016**, *16*, 82–99. [CrossRef]
44. Jaisakthi, S.A.; Chandrabose, A.; Mirunalini, P. Automatic skin lesion segmentation using semi-supervised learning technique. *arXiv* **2017**, arXiv:1703.04301.
45. Lynn, N.C.; Kyu, Z.M. Segmentation and classification of skin cancer melanoma from skin lesion images. In Proceedings of the 2017 18th International Conference on Parallel and Distributed Computing, Applications and Technologies (PDCAT), Taipei, Taiwan, 18–20 December 2017.
46. Amin, J.; Anjum, M.A.; Sharif, M.; Kadry, S.; Nam, Y.; Wang, S. Convolutional Bi-LSTM based human gait recognition using video sequences. *Comput. Mater. Contin.* **2021**, *68*, 2693–2709. [CrossRef]
47. Albahar, M.A. Skin lesion classification using convolutional neural network with novel regularizer. *IEEE Access* **2019**, *7*, 38306–38313. [CrossRef]
48. Milton, M.A.A. Automated skin lesion classification using ensemble of deep neural networks in ISIC 2018: Skin lesion analysis towards melanoma detection challenge. *arXiv* **2019**, arXiv:1901.10802.
49. Linsky, T.W.; Vergara, R.; Codina, N.; Nelson, J.W.; Walker, M.J.; Su, W.; Barnes, C.O.; Hsiang, T.-Y.; Esser-Nobis, K.; Yu, K. De novo design of potent and resilient hACE2 decoys to neutralize SARS-CoV-2. *Science* **2020**, *370*, 1208–1214. [CrossRef] [PubMed]
50. Zhang, J.; Xie, Y.; Xia, Y.; Shen, C. Attention residual learning for skin lesion classification. *IEEE Trans. Med. Imaging* **2019**, *38*, 2092–2103. [CrossRef]
51. Sandler, M.; Howard, A.; Zhu, M.; Zhmoginov, A.; Chen, L.-C. Mobilenetv2: Inverted residuals and linear bottlenecks. In Proceedings of the IEEE Conference on Computer Vision and Pattern Recognition, Salt Lake City, UT, USA, 18–22 June 2018.
52. Chen, L.-C.; Zhu, Y.; Papandreou, G.; Schroff, F.; Adam, H. Encoder-decoder with atrous separable convolution for semantic image segmentation. In Proceedings of the European Conference on Computer Vision (ECCV), Munich, Germany, 8–14 September 2018.
53. Nalini, M.; Radhika, K. Comparative analysis of deep network models through transfer learning. In Proceedings of the 2020 Fourth International Conference on I-SMAC (IoT in Social, Mobile, Analytics and Cloud)(I-SMAC), Palladam, India, 7–9 October 2020.
54. Huang, G.; Liu, Z.; Van Der Maaten, L.; Weinberger, K.Q. Densely connected convolutional networks. In Proceedings of the IEEE Conference on Computer Vision and Pattern Recognition, Honolulu, HI, USA, 21–26 July 2017.
55. Li, S.; Chen, H.; Wang, M.; Heidari, A.A.; Mirjalili, S. Slime mould algorithm: A new method for stochastic optimization. *Future Gener. Comput. Syst.* **2020**, *111*, 300–323. [CrossRef]
56. Wazery, Y.M.; Saber, E.; Houssein, E.H.; Ali, A.A.; Amer, E. An efficient slime mould algorithm combined with k-nearest neighbor for medical classification tasks. *IEEE Access* **2021**, *9*, 113666–113682. [CrossRef]

57. Pereira, F.; Mitchell, T.; Botvinick, M. Machine learning classifiers and fMRI: A tutorial overview. *Neuroimage* **2009**, *45*, S199–S209. [CrossRef]
58. Singh, S.; Kumar, R. Histopathological image analysis for breast cancer detection using cubic SVM. In Proceedings of the 2020 7th International Conference on Signal Processing and Integrated Networks (SPIN), Noida, India, 27–28 February 2020.
59. Ali, A.; Alrubei, M.; Hassan, L.; Al-Ja'afari, M.; Abdulwahed, S. Diabetes classification based on KNN. *IIUM Eng. J.* **2020**, *21*, 175–181. [CrossRef]
60. Subbarao, M.V.; Samundiswary, P. Performance analysis of modulation recognition in multipath fading channels using pattern recognition classifiers. *Wirel. Pers. Commun.* **2020**, *115*, 129–151. [CrossRef]
61. Gutman, D.; Codella, N.C.; Celebi, E.; Helba, B.; Marchetti, M.; Mishra, N.; Halpern, A. Skin lesion analysis toward melanoma detection: A challenge at the international symposium on biomedical imaging (ISBI) 2016, hosted by the international skin imaging collaboration (ISIC). *arXiv* **2016**, arXiv:1605.01397.
62. Codella, N.C.; Gutman, D.; Celebi, M.E.; Helba, B.; Marchetti, M.A.; Dusza, S.W.; Kalloo, A.; Liopyris, K.; Mishra, N.; Kittler, H. Skin lesion analysis toward melanoma detection: A challenge at the 2017 international symposium on biomedical imaging (isbi), hosted by the international skin imaging collaboration (isic). In Proceedings of the 2018 IEEE 15th International Symposium on Biomedical Imaging (ISBI 2018), Washington, DC, USA, 4–7 April 2018.
63. Codella, N.; Rotemberg, V.; Tschandl, P.; Celebi, M.E.; Dusza, S.; Gutman, D.; Helba, B.; Kalloo, A.; Liopyris, K.; Marchetti, M. Skin lesion analysis toward melanoma detection 2018: A challenge hosted by the international skin imaging collaboration (isic). *arXiv* **2019**, arXiv:1902.03368.
64. Mendonça, T.; Ferreira, P.M.; Marques, J.S.; Marcal, A.R.; Rozeira, J. PH 2-A dermoscopic image database for research and benchmarking. In Proceedings of the 2013 35th Annual International Conference of the IEEE Engineering in Medicine and Biology Society (EMBC), Osaka, Japan, 3–7 July 2013.
65. Ünver, H.M.; Ayan, E. Skin lesion segmentation in dermoscopic images with combination of YOLO and grabcut algorithm. *Diagnostics* **2019**, *9*, 72. [CrossRef]
66. Tschandl, P.; Rosendahl, C.; Kittler, H. The HAM10000 dataset, a large collection of multi-source dermatoscopic images of common pigmented skin lesions. *Sci. Data* **2018**, *5*, 180161. [CrossRef] [PubMed]
67. Combalia, M.; Codella, N.C.; Rotemberg, V.; Helba, B.; Vilaplana, V.; Reiter, O.; Carrera, C.; Barreiro, A.; Halpern, A.C.; Puig, S. Bcn20000: Dermoscopic lesions in the wild. *arXiv* **2019**, arXiv:1908.02288.
68. Giotis, I.; Molders, N.; Land, S.; Biehl, M.; Jonkman, M.F.; Petkov, N. MED-NODE: A computer-assisted melanoma diagnosis system using non-dermoscopic images. *Expert Syst. Appl.* **2015**, *42*, 6578–6585. [CrossRef]
69. Hosny, K.M.; Kassem, M.A.; Foaud, M.M. Classification of skin lesions using transfer learning and augmentation with Alex-net. *PloS ONE* **2019**, *14*, e0217293. [CrossRef] [PubMed]
70. Le, P.T.; Chang, C.-C.; Li, Y.-H.; Hsu, Y.-C.; Wang, J.-C. Antialiasing Attention Spatial Convolution Model for Skin Lesion Segmentation with Applications in the Medical IoT. *Wirel. Commun. Mob. Comput.* **2022**, *2022*, 1278515. [CrossRef]
71. Tong, X.; Wei, J.; Sun, B.; Su, S.; Zuo, Z.; Wu, P. ASCU-Net: Attention gate, spatial and channel attention u-net for skin lesion segmentation. *Diagnostics* **2021**, *11*, 501. [CrossRef] [PubMed]
72. Xie, F.; Yang, J.; Jiang, Z.; Zheng, Y.; Wang, Y. Skin lesion segmentation using high-resolution convolutional neural network. *Comput. Methods Programs Biomed.* **2020**, *186*, 105241. [CrossRef]
73. Bi, L.; Kim, J.; Ahn, E.; Kumar, A.; Feng, D.; Fulham, M. Step-wise integration of deep class-specific learning for dermoscopic image segmentation. *Pattern Recognit.* **2019**, *85*, 78–89. [CrossRef]
74. Shan, P.; Wang, Y.; Fu, C.; Song, W.; Chen, J. Automatic skin lesion segmentation based on FC-DPN. *Comput. Biol. Med.* **2020**, *123*, 103762. [CrossRef]
75. Kaymak, R.; Kaymak, C.; Ucar, A. Skin lesion segmentation using fully convolutional networks: A comparative experimental study. *Expert Syst. Appl.* **2020**, *161*, 113742. [CrossRef]
76. Al-Masni, M.A.; Al-Antari, M.A.; Choi, M.-T.; Han, S.-M.; Kim, T.-S. Skin lesion segmentation in dermoscopy images via deep full resolution convolutional networks. *Comput. Methods Programs Biomed.* **2018**, *162*, 221–231. [CrossRef] [PubMed]
77. Khouloud, S.; Ahlem, M.; Fadel, T.; Amel, S. W-net and inception residual network for skin lesion segmentation and classification. *Appl. Intell.* **2022**, *52*, 3976–3994. [CrossRef]
78. Arora, R.; Raman, B.; Nayyar, K.; Awasthi, R. Automated skin lesion segmentation using attention-based deep convolutional neural network. *Biomed. Signal Process. Control.* **2021**, *65*, 102358. [CrossRef]
79. Bi, L.; Feng, D.; Kim, J. Improving automatic skin lesion segmentation using adversarial learning based data augmentation. *arXiv* **2018**, arXiv:1807.08392.
80. Jahanifar, M.; Tajeddin, N.Z.; Koohbanani, N.A.; Gooya, A.; Rajpoot, N. Segmentation of skin lesions and their attributes using multi-scale convolutional neural networks and domain specific augmentations. *arXiv* **2018**, arXiv:1809.10243.
81. Chen, P.; Huang, S.; Yue, Q. Skin Lesion Segmentation Using Recurrent Attentional Convolutional Networks. *IEEE Access* **2022**, *10*, 94007–94018. [CrossRef]
82. Zhang, G.; Shen, X.; Chen, S.; Liang, L.; Luo, Y.; Yu, J.; Lu, J. DSM: A deep supervised multi-scale network learning for skin cancer segmentation. *IEEE Access* **2019**, *7*, 140936–140945. [CrossRef]
83. Pacheco, A.G.; Ali, A.-R.; Trappenberg, T. Skin cancer detection based on deep learning and entropy to detect outlier samples. *arXiv* **2019**, arXiv:1909.04525.

84. Setiawan, A.W. Effect of Color Enhancement on Early Detection of Skin Cancer using Convolutional Neural Network. In Proceedings of the 2020 IEEE International Conference on Informatics, IoT, and Enabling Technologies (ICIoT), Doha, Qatar, 2–5 February 2020.
85. Pacheco, A.G.; Sastry, C.S.; Trappenberg, T.; Oore, S.; Krohling, R.A. On out-of-distribution detection algorithms with deep neural skin cancer classifiers. In Proceedings of the IEEE/CVF Conference on Computer Vision and Pattern Recognition Workshops, Seattle, WA, USA, 14–19 June 2020.
86. Saarela, M.; Geogieva, L. Robustness, Stability, and Fidelity of Explanations for a Deep Skin Cancer Classification Model. *Appl. Sci.* **2022**, *12*, 9545. [CrossRef]
87. Afza, F.; Sharif, M.; Mittal, M.; Khan, M.A.; Hemanth, D.J. A hierarchical three-step superpixels and deep learning framework for skin lesion classification. *Methods* **2022**, *202*, 88–102. [CrossRef]
88. Khan, M.A.; Akram, T.; Zhang, Y.-D.; Sharif, M. Attributes based skin lesion detection and recognition: A mask RCNN and transfer learning-based deep learning framework. *Pattern Recognit. Lett.* **2021**, *143*, 58–66. [CrossRef]
89. Khan, M.A.; Javed, M.Y.; Sharif, M.; Saba, T.; Rehman, A. Multi-model deep neural network based features extraction and optimal selection approach for skin lesion classification. In Proceedings of the 2019 International Conference on Computer and Information Sciences (ICCIS), Sakaka, Saudi Arabia, 3–4 April 2019.
90. Hosny, K.M.; Kassem, M.A. Refined residual deep convolutional network for skin lesion classification. *J. Digit. Imaging* **2022**, *35*, 258–280. [CrossRef]
91. Alizadeh, S.M.; Mahloojifar, A. Automatic skin cancer detection in dermoscopy images by combining convolutional neural networks and texture features. *Int. J. Imaging Syst. Technol.* **2021**, *31*, 695–707. [CrossRef]
92. Kumar, M.; Alshehri, M.; AlGhamdi, R.; Sharma, P.; Deep, V. A de-ann inspired skin cancer detection approach using fuzzy c-means clustering. *Mob. Netw. Appl.* **2020**, *25*, 1319–1329. [CrossRef]
93. Arora, G.; Dubey, A.K.; Jaffery, Z.A.; Rocha, A. Bag of feature and support vector machine based early diagnosis of skin cancer. *Neural Comput. Appl.* **2020**, *34*, 8385–8392. [CrossRef]
94. Xie, Y.; Zhang, J.; Xia, Y.; Shen, C. A mutual bootstrapping model for automated skin lesion segmentation and classification. *IEEE Trans. Med. Imaging* **2020**, *39*, 2482–2493. [CrossRef]
95. Gerges, F.; Shih, F.Y. A Convolutional Deep Neural Network Approach for Skin Cancer Detection Using Skin Lesion Images. *Int. J. Electr. Comput. Eng.* **2021**, *15*, 475–478.
96. Mukherjee, S.; Adhikari, A.; Roy, M. Malignant melanoma detection using multi layer preceptron with visually imperceptible features and PCA components from MED-NODE dataset. *Int. J. Med. Eng. Inform.* **2020**, *12*, 151–168. [CrossRef]